OXFORD

BRIEF REPORT

A Pediatric Intra-Axial Malignant *SMARCB1*-Deficient Desmoplastic Tumor Arising in Meningioangiomatosis

Sabrina Rossi, MD, PhD, Monica Brenca, PhD, Lucia Zanatta, PhD, Elena Trincia, MD,
Angela Guerriero, MD, Cristina Pizzato, MD, Alessandro Fiorindi, MD, PhD, Elisabetta Viscardi, MD,
Felice Giangaspero, MD, Roberta Maestro, PhD, Angelo Paolo Dei Tos, MD, and
Caterina Giannini, MD, PhD

Abstract

SMARCB1 inactivation is a well-established trigger event in atypical teratoid/rhabdoid tumor. Recently, a role for *SMARCB1* inactivation has emerged as a mechanism of clonal evolution in other tumor types, including rare brain tumors. We describe an unusual malignant intra-axial *SMARCB1*-deficient spindle cell desmoplastic neoplasm, occurring in a 6-year-old child with meningioangiomatosis and a long history of seizures. Striking features of the tumor were a storiform pattern and strong CD34 expression. Undifferentiated round cell areas with isolated rhabdoid cells showing high mitotic index and focal necrosis with INI1 expression loss were present. The meningioangiomatosis component showed few chromosomal imbalances, including chromosomal 22 monosomy (where *SMARCB1* maps) and gain at 6q14.3. In addition to these abnormalities, the spindle cell desmoplastic neoplasm and its dedifferentiated *SMARCB1*-deficient component shared several other aberrations, including homozygous deletion at 9p21.3, losses at 1p, 3p, 3q, 10p, and 13q, gains and losses at 5p and 11p. In line with INI1 loss, the dedifferentiated component showed remarkably decreased levels of SMARCB1 transcript. The residual *SMARCB1* allele was wildtype. Our findings suggest progression from the meningioangiomatosis to the malignant desmoplastic neoplasm through the occurrence of complex chromosomal abnormalities, and point to functional silencing of *SMARCB1* in the dedifferentiation component.

Key Words: Brain, Dedifferentiation, INI1-loss, Meningioangiomatosis, Pediatric, Sarcoma, SMARCB1 inactivation.

INTRODUCTION

The *SMARCB1* tumor suppressor gene, located on chromosome 22q11.2, encodes a core subunit (INI1) of the SWI/SNF complex that is involved in chromatin remodeling and transcriptional regulation [1]. Inactivation of *SMARCB1*, resulting in loss of expression of the encoded INI1 protein, is typically considered a trigger event in atypical teratoid/rhabdoid tumors occurring in the central nervous system (CNS) [1]. It is also involved in tumor progression in other tumor types such as KRAS-mutated pancreatic cancers and microsatellite unstable colorectal cancers [2].

A role for *SMARCB1* has been recently reported in the progression-associated tumor dedifferentiation for rare cases of CNS tumors, including pleomorphic xantoastrocytomas (PXA) (4 cases), gangliogliomas (2 cases), high-grade gliomas (5 cases), ependymoma (1 case), and meningioma (1 case) [3–14].

Meningioangiomatosis is a rare benign leptomeningeal and intracortical lesion characterized by the presence of numerous variably hyalinized small blood vessels surrounded by a spindle cell proliferation and occasional association with meningioma has been reported [15]. The nature of meningioangiomatosis is still not clear and there has been long debate whether it is a neoplastic or a reactive/hamartomatous process [15, 16].

We herein describe a very unusual malignant pediatric intra-axial spindle cell desmoplastic neoplasm with focal *SMARCB1* inactivation arising in a background of meningioangiomatosis.

MATERIALS AND METHODS

Immunohistochemistry

Immunohistochemistry was carried out on formalin-fixed paraffin-embedded sections representing the 3 different

tissue components using an automated immunostainer (Dako Omnis, DAKO, Glostrup, Denmark). Primary antibodies directed against the following antigens were applied: CD34 (clone QBEnd-10, prediluted, high pH, DAKO), smooth muscle actin (clone 1A4, prediluted, high pH, DAKO), GFAP (prediluted, high pH, DAKO), vimentin (clone V9, prediluted, high pH, DAKO), OLIG2 (211F1.1, prediluted, high pH, Cell Marque, Darmstadt, Germany), S100 (prediluted, high pH, DAKO), SOX10 (EP268, 1/100, high pH, Cell Marque), NeuN (1/2000 high pH, DBA, Aachen, Germany), Synaptophysin (clone DAK-SYNAP, prediluted, high pH, DAKO), neurofilament (clone 2F11, prediluted, high pH, DAKO), desmin (clone D33, prediluted, high pH, DAKO), caldesmon (clone H-CD, prediluted, high pH, DAKO), miogenin (clone FD5, prediluted, high pH, DAKO), L1CAM (clone UJ127.11, 1/100, high pH, Sigma Aldrich, St. Louis, MO), progesterone receptor (clone 636, prediluted, high pH, DAKO), STAT6 (1/1000, high pH, Santa Cruz Biotechnology, Santa Cruz, CA), p53 (clone DO-7, prediluted, high pH, DAKO), IDH1R132H (clone DIA H09, 1/100, high pH, Dianova, Hamburg, Germany), BRAF V600E (clone VE1, 1/100, high pH, Spring Bioscience Corp., Pleasanton, CA), H3.3K27M (1/1500, high pH, Millipore, Darmstadt, Germany), ATRX (1/100, high pH, Sigma Aldrich), H3.3K27me3 (1/100, high pH, Millipore), INI1 (1/25, high pH, BD Bioscience, San Jose, CA), BRG1 (1/100, high pH, Millipore), EMA (clone E29, prediluted, high pH, DAKO), cytokeratinCAM5.2 (1/10, high pH, BD Bioscience).

Chromosomal Microarray

Chromosomal microarray analysis was carried out on the 3 different components of the specimen: Fragments entirely consisting of meningioangiomatosis, fragments of desmoplastic spindle cell tumor, and *SMARCB1*-deficient dedifferentiated areas isolated by dissection. Copy number variation and copy neutral loss of heterozygosity were detected using OncoScan assay kits (Affymetrix, Santa Clara, CA), as previously described (14).

RNA Extraction and qRT-PCR Analysis

Also qRT-PCR was performed separately on the 3 different components of the specimen. Total RNA was extracted as previously described and reverse transcribed into cDNA using the SuperScript III Reverse Transcriptase (Life Technologies, Monza, Italy), according to the supplier's protocol. qRT-PCR was performed with SSO Fast EvaGreen Supermix (Bio-Rad, Milano, Italy). Expression analysis of SMARCB1 was carried out with qRT-PCR on a CFX96 Real-Time Apparatus (Bio-Rad). SMARCB1 relative expression levels were calculated by using the comparative Ct (ΔCt) method and the geometric average of 3 housekeeping genes (SF3A1, B2M, ACTB) using the following primers:

SMARCB1: Fw-GGGGAGTTTGTCACCACCAT; Rev-CG GATGGCAATCTCCACTGT
SF3A1: Fw-ACCTTCTAAGCCAGTTGTGGG; Rev-TAGC TTCAAATTCAGGCCCGT

ACTB: Fw-CACCTTCTACAATGAGCTGCGT; Rev-AGC CTGGATAGCAACGTACATG
B2M: Fw-GAGTATGCCTGCCGTGTG; Rev-AATCCAAA TGCGGCATCT

SMARCB1 Mutation Analysis

SMARCB1 mutation analyses were carried out on the dedifferentiated SMARCB1-deficient component by exons amplification and Sanger sequencing. DNA was extracted using the QIAamp DNA FFPE Tissue Kit (Qiagen), according to manufacturer instructions. The primers reported in reference (17) were used for the analysis of the 9 SMARCB1 coding exons with the exception of the following forward primer for the exon 4 that was changed: GATCAGGCTCCTATACT-GAC. PCR conditions are available upon request. PCR products were enzymatically purified by IllustraExoProStar PCR Product Cleanup Reagent (GE Healthcare Bio-Sciences, Pittsburgh, PA) and then sequenced with BigDye Terminator chemistry (Thermo Fisher, Waltham, MA).

Case History

A 6-year-old girl presented with a brief episode of loss of consciousness followed by aggressive behavior, psychomotor impairment and walking instability. She had a long history of focal seizures from the age of 16 months, intellectual disability and dysfunctional behavior. She was known to have a right occipital cortical lesion radiologically interpreted as nodular dysplasia with associated multiple "subcortical cysts" in the ipsilateral temporo-parietal region (Fig. 1A–C). For this lesion the girl started a therapy for epilepsy and was followed by periodical MRI and electroencephalography from the age of 16 months until the age of 24 months and only by periodical electroencephalography from the age of 24 months. She had no family history of neoplastic or genetic disease. An MRI performed at age 6 revealed 2 lesions, both intra-axial: A large (7.8 × 7 cm) enhancing mass in the right temporal region and a separate, smaller (1.8 × 1.5 cm) enhancing nodule in the ipsilateral occipital lobe at the site of the previously described nodular dysplastic lesion (Fig. 1D, E). The temporal mass featured a solid and a cystic component with focal calcifications and was surrounded by white matter edema with midline shift. The occipital nodule was mostly solid with a minimal cystic component. Gross total surgical resection of the temporal tumor was performed, which disclosed a CD34-positive malignant spindle cell desmoplastic neoplasm with focal INI1-loss in a background of meningioangiomatosis. Because of these findings, the possibility of a rhabdoid tumor predisposition syndrome or neurofibromatosis type 2 was considered, but neither SMARCB1 nor NF2 germline mutations were found.

Removal of the occipital lesion was planned before starting adjuvant treatment, but 2 months after surgery additional imaging showed rapid regrowth of the temporal neoplasm along the posterior portion of the tumor (2.4 × 0.7 cm), and the occipital mass had increased to 3.5 × 3 cm. The patient underwent a second surgery with gross total resection of both lesions, and started treatment with a multimodal therapy protocol (EU-RHAB-2010).
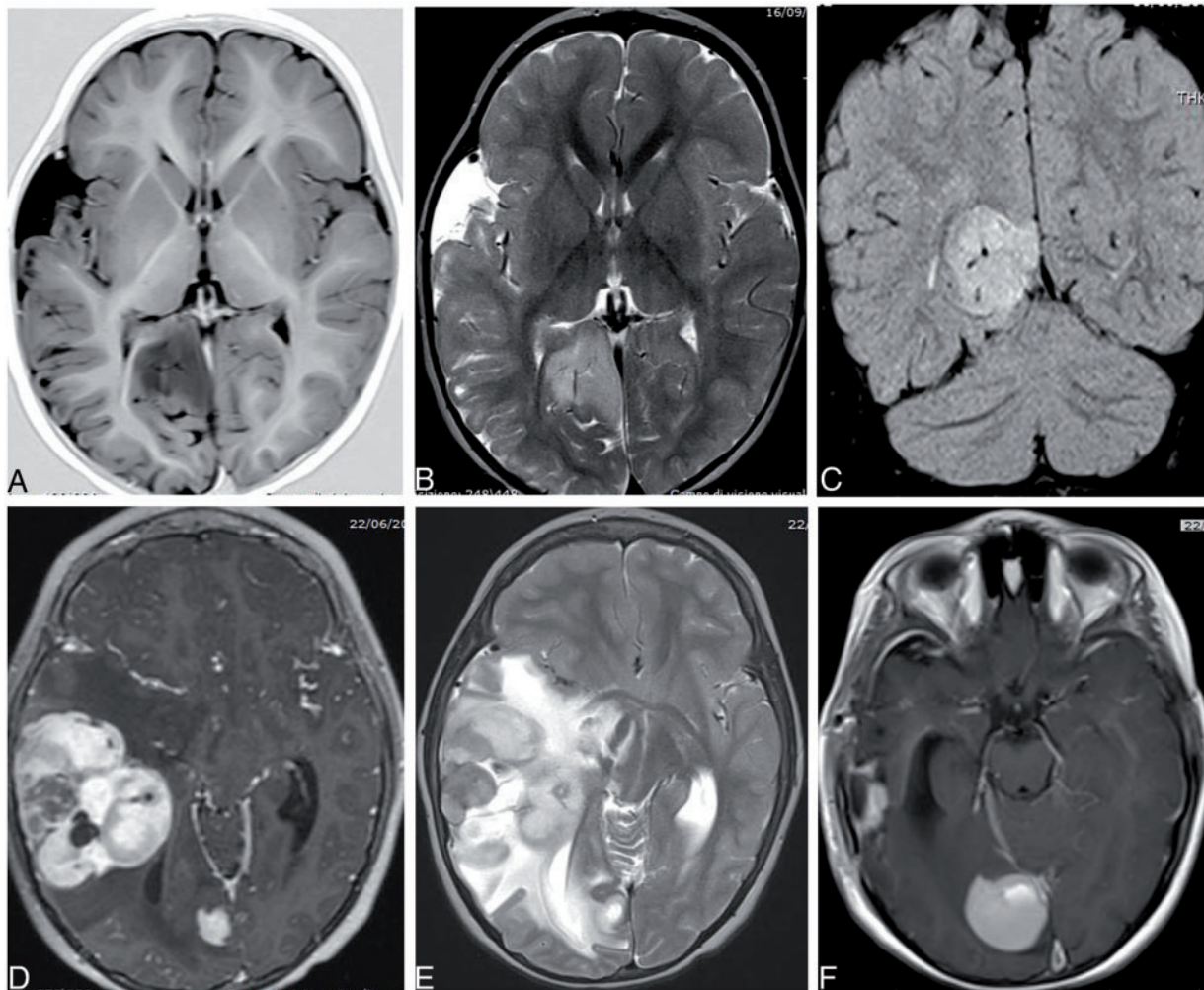
FIGURE 1. MRI performed at 16 months showed a cortical lesion involving the right occipital lobe, which appeared hypointense on the axial inversion recovery T1-weighted image **(A)**, and hyperintense on the axial T2-weighted image **(B)**, and coronal (T2-weighted) flair image **(C)**. The ipsilateral temporo-parietal cortical and subcortical layers were abnormal with blurring of the white-grey junction and multiple subcortical cysts **(A, B)**. A MRI obtained at age 6 showed a 7.5 × 7 cm right temporo-parietal intra-axial enhancing tumor with a solid and a cystic component and a separate 1.8 × 1.5 cm occipital intra-axial enhancing lesion **(D)**. Both the tumors were hyperintense in the T2-weighted image **(E)**. Two months after the gross total resection of the temporal lesion, a new MRI showed a remarkable increase of the occipital lesion (3.5 × 3 cm) and tumor regrowth at the prior surgical site (2.4 × 0.7 cm) **(F)**.

Three months later, MRI showed a new temporal tumor recurrence and radiotherapy was commenced (sooner than originally scheduled). Because of further tumor progression, the treatment was suspended 3 months later (7 months from therapy initiation). The patient died 14 months from first diagnosis.

Pathology

The temporal and the occipital lesions appeared firm and translucent at macroscopic examination. Histologically, both tumors were heterogeneous. Their core was strikingly desmoplastic and consisted of spindle cells arranged in a storiform pattern with a variable degree of cellularity, nuclear atypia and mitotic activity (Fig. 2A). Hypocellular areas

featuring mild nuclear atypia and low mitotic index (2/10 HPF) were mixed with hypercellular areas with remarkable nuclear pleomorphism and brisk mitotic activity (up to 20/10 HPF; Fig. 2B, C). The lesions infiltrated the cerebral parenchyma and extended along the perivascular Virchow-Robin spaces. Notably, the peripheral parts of the tumors merged gradually with areas of the cortex showing extensively hyalinized vessels surrounded by bland spindle cells, focal psammoma bodies, consistent with meningioangiomatosis (Fig. 2D, E). Both neoplasms showed a strong expression of vimentin and CD34 and focal smooth muscle actin. Glial markers (GFAP, OLIG2, S100, SOX10), neural markers (NeuN, synaptophysin, neurofilament), muscular markers (desmin, caldesmon, myogenin), L1CAM, progesterone receptor and STAT6 were negative. p53 was expressed in
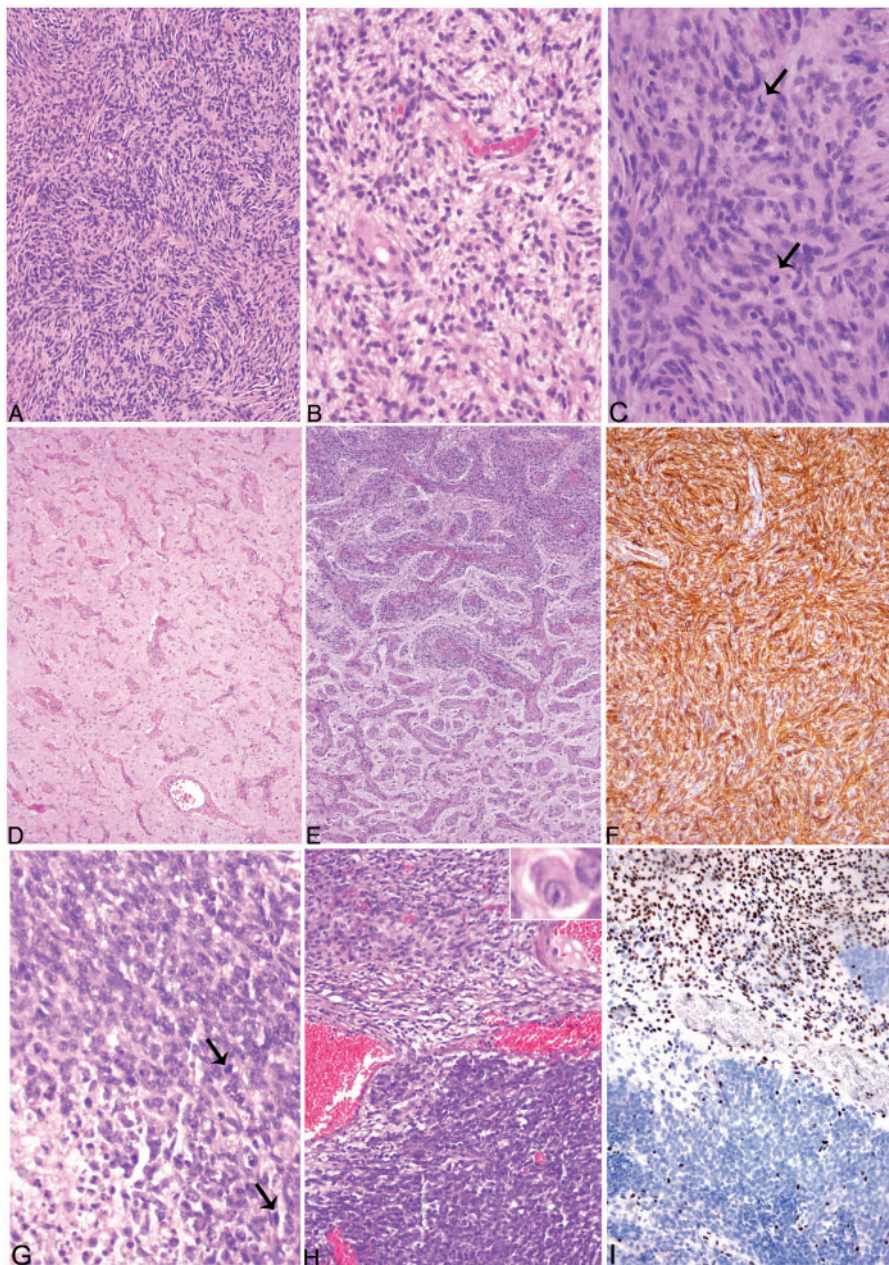
885

FIGURE 2. The desmoplastic spindle cell component showed a storiform pattern of growth **(A)** and was characterized by both bland hypocellular areas with low mitotic index **(B)** and hypercellular areas with nuclear atypia and high mitotic index (**C**, arrows indicate mitoses). Associated with the tumor there were very hypocellular areas featuring hyalinized vessels surrounded by a bland spindle cell proliferation, consistent with meningioangiomatosis **(D)**. Areas of morphological transitions from the meningioangiomatosis to perivascular hypercellular proliferation of clear-cut neoplastic cells invading the Virchow-Robin spaces could be identified at the edge of the tumor **(E)**. The desmoplastic spindle cell component was diffusely and strongly positive for CD34 **(F)**. Only in the temporal lesion, there were foci of undifferentiated tumor featuring cells with high nuclear-cytoplasmic ratio and prominent nucleoli with necrosis (**G**, arrows indicate mitoses). A focus of undifferentiated tumor (bottom) juxtaposed to the desmoplastic spindle cell component (top) can be observed in this picture **(H)**. Isolated rhabdoid cells were present in the undifferentiated component (**H**, inset). INI1 loss of expression was confined to the undifferentiated part of the tumor **(I)**.

∼20% of neoplastic cells. IDH1 R132H, BRAF V600E, H3.3K27M were negative, whereas expression of ATRX, H3.3K27me3, INI1, and BRG1 were homogeneously retained.

Only in the temporal tumor an undifferentiated component with small round cells and isolated rhabdoid elements was present focally in the first resection (<10%) and widespread in the recurrence (>50%). Mitotic index was very high

(40/10 HPF) and necrosis was present focally (Fig. 1E, F). This component showed loss of INI1 expression and focal EMA, smooth muscle actin and cytokeratin (CAM5.2) immunostaining (Fig. 1G). The tumors were wild-type for *H3F3A* and *TERT* promoter by PCR. No rearrangements of *ETV6* and *PDGFB* were found by FISH analysis.

Molecular Analyses

Molecular analyses were carried out separately on meningioangiomatosis, the spindle cell desmoplastic neoplasm and its dedifferentiated *SMARCB1*-deficient component.

The meningioangiomatosis showed only 3 chromosomal imbalances: 22 monosomy (where *SMARCB1* gene maps), 6q14.3 gain, both shared with the desmoplastic tumor and its dedifferentiated *SMARCB1*-deficient component, and a loss at 5q, which was unique to this component. The chromosomal imbalances of the spindle cell desmoplastic neoplasm and the dedifferentiated *SMARCB1*-deficient component overlapped almost completely. In addition to the monosomy for chromosome 22 and the gain at 6q14.3, they both showed homozygous deletion at 9p21.3 (CDKN2A), losses at 1p, 3p, 3q, 10p, and 13q, and gains and losses at 5p and 11p. A gain at the X chromosome was present only in the dedifferentiated component (Supplementary Data Fig. S1).

The dedifferentiated SMARCB1-deficient component displayed dramatically reduced SMARCB1 mRNA expression levels compared with the spindle cell desmoplastic neoplasm, in line with INI1 loss of expression observed by immunohistochemistry.

No mutation in the coding sequence of the *SMARCB1* gene was detected in the dedifferentiated component.

Ultrastructure

We performed ultrastructural studies from the paraffin-embedded tissue, which resulted in moderate tissue preservation. In the meningioangiomatosis component we identified vessels with dense collagen deposition and scant perivascular cells with no distinctive morphology. The spindle cell component showed dense extracellular collagen deposition consistent with the remarkable desmoplasia observed histologically. No distinctive features could be identified in the cells. There were no features to suggest either a glial or a meningothelial origin (Supplementary Data Fig. S2).

DISCUSSION

We herein described a case of a pediatric intra-axial composite tumor consisting of a malignant spindle cell desmoplastic neoplasm with focal INI1 loss consistent with tumor progression/dedifferentiation.

Tumor progression associated to *SMARCB1* inactivation/INI1 loss is uncommon in CNS tumors. To the best of our knowledge, only 13 such cases have been reported (3–14). The line of differentiation of the "parent" tumor is mostly astrocytic (4 PXA, 5 high-grade gliomas/GBMs), with only 1 meningeal and 1 ependymal case described (3–14).

The case reported here is quite unusual, as the "parent" tumor is difficult to classify. The location was intra-axial according to both radiological and surgical presentation. Clinical and radiological work-up excluded its metastatic nature. The tumor consisted of spindle cells arranged in a storiform growth pattern, expressing vimentin, CD34 and focal smooth muscle actin. A glial component was not identified either histologically or by immunohistochemistry (GFAP, OLIG2, and SOX10 were negative). Likewise, there was no evidence of meningothelial differentiation by hematoxylin and eosin, immunohistochemical and ultrastructural analyses. Despite the remarkable CD34 expression, STAT6 was completely negative, arguing against anaplastic solitary fibrous tumor/hemangiopericytoma. Finally, the absence of *ETV6* rearrangement as well as the diffuse expression of CD34 made the possibility of infantile fibrosarcoma very unlikely. In the end, the tumor was classified as spindle cell desmoplastic tumor NOS. It could most likely be a sarcoma, although primary intracranial sarcomas are extremely rare, with very few and old studies conducted on histologically heterogeneous series (18).

The *SMARCB1*-deficient dedifferentiated component was very limited in extension in the primary temporal mass and largely represented in the relapsing lesion, which, despite multimodal therapy, led to the patient's death. This suggests that INI1 loss is a secondary event associated with clonal evolution, underlying the rapid clinical recurrence/progression. Analogous with our case, the majority of the cases of *SMARCB1* inactivation/INI1 loss-associated dedifferentiation reported in the literature featured a very aggressive clinical behavior (Table).

Intriguingly, the chromosomal microarray of the "parent" neoplasm and the SMARCB1-deficient component were essentially identical. In particular, both lesions were monosomic for chromosome 22, where the *SMARCB1* gene maps. Despite retention of a *SMARCB1* wild type allele, the dedifferentiated component showed dramatically reduced SMARCB1 mRNA expression levels compared with the "parent" tumor, correlating with the INI1 loss of expression by immunohistochemistry. A similar scenario has been recently reported in a case of RELA-rearranged ependymoma showing areas of *SMARCB1* loss-associated dedifferentiation (11). Also in this case the 2 components showed an identical chromosomal array profile, including loss of 1 copy of chromosome 22 and no additional *SMARCB1* gene mutation. Overall, in both ours and this latter case, the dedifferentiated component retains a *SMARCB1* wild type allele suggesting that INI1 loss-associated dedifferentiation may rely on functional gene silencing. This hypothesis, although yet to be proven, would be in line with the mounting evidence supporting a role for epigenetic deregulation in the pathogenesis of pediatric cancer. In fact, although compared with the adult counterpart the mutational load is reduced in pediatric tumors, they show remarkably high frequency alterations affecting epigenetic regulators (e.g. mutations in histone H3 in midline high-grade gliomas) (19, 20).

Interestingly, in this case the temporal and occipital tumors developed within a diffuse area of meningioangiomatosis, originally interpreted as cortical dysplasia. Of note, neither radiation therapy nor chemotherapy was administered for this lesion, ruling out the possibility of a treatment-induced malignant transformation. Meningioangiomatosis is a rare

TABLE. CNS Tumors With Dedifferentiation Associated With *SMARCB1*-Inactivation Described in the Literature and the Current Case

Literature Cases				"Parent" Tumor		Dedifferentiated Component			
Reference	Age/Sex	Site	Outcome, Time to Death From Dedifferentiation	Histotype	Driver Alteration	Rhabdoid Morphology	INI1 Loss	22q Loss	SMARCB1 Somatic Mutation
5	23/M	Right F	DOC, 6 weeks (pneumonia)	PXA	BRAF V600E	Y	Y	Y	Y
7	8/F	Right F	NA	PXA	BRAF V600E	Y	Y	NA	NA
8	13/F	Cerebellum	DOD, 5 months	PXA	BRAF V600E	Y	Y	NA	NA
14	NA	NA	NA	PXA	BRAF V600E	Y	Y	Y	NA
3*	11/M	Optic pathway	DOD, 12 months	Ganglioglioma	BRAF V600E	Y	Y	NA	Y
4	6/M	Right P	DOD, 2 weeks	Ganglioglioma	BRAF V600E	Y	Y	Y	Y (homoz. microdel)
10	22/F	Right O	DOD, 5 months	High grade glioma	NA	Y	Y	NA	NA
6	67/F	Right P-O	DOD, 9 months	GBM	PTEN loss EGFR amplification	Y	Y	Y	NA
	18/M	Right F	DOD, 5 months	GBM	NA	Y	Y	Y (subclonal)	NA
9	27/F	Left O	DOD, 1 month	GBM	NA	Y	Y	Y	NA
12*	7/F	Left T-P	DOD, 13 months	GBM	NA	Y	Y	NA	Y (homoz. del)
11[†]	24/M	Left F	NED, 30 months	Ependymoma	C11orf95-RELA	Y	Y	Y	N
13	7/M	Right T	NED, 30 months	Meningioma	NA	Y	Y	NA	NA

Our Case				"Parent" Tumor		Dedifferentiated Component			
	Age/Sex	Site	Outcome, Time to Death	Histotype	Driver Alteration	Rhabdoid Morphology	INI1 Loss	22q Loss	SMARCB1 Somatic Mutation
Current report[†]	6/F	Right T-P-O	DOD, 14 months	Malignant desmoplastic spindle cell tumor	NA	Isolated cells	Y		Y	N

F, frontal; P, parietal; O, occipital; T, temporal; DOD, dead of disease; NED, no evidence of disease; Y, yes; N, no; NA, not assessed.

*In these 2 cases, the parent and the INI1-deficient tumor were not concomitant; the latter developed in the tumor bed 9 years[3] and 17 months[12] after GTR of the parent tumor followed by RT and CT.

[†]In these cases, 22 loss was seen in both the dedifferentiated component and in the parent tumor.

benign leptomeningeal and intracortical plaque-like lesion defined by the presence of numerous small blood vessels surrounded by a spindle cell proliferation with a variable degree of cellularity, hyalinization and calcification (15). It may be occasionally associated with meningioma (15). Meningioangiomatosis may be sporadic or develop in the context of neurofibromatosis type 2 (NF-type 2). It may cause seizures, especially in the sporadic form, but may also be asymptomatic. Our patient did not have a personal and/or familial history of NF-type 2 and did not carry *NF2* germline mutation. Although we cannot exclude the possibility of mosaicism for *NF2* mutation, the patient's long history of seizures is coherent with a sporadic form.

The nature of meningioangiomatosis is still elusive and there has been long debate on its neoplastic versus reactive/hamartomatous origin (15, 16). In our case, multiple lines of evidence support the premalignant nature of the

meningioangiomatosis. First, the patient had a long clinical history of seizures and the cortical alterations were radiologically documented 4 years earlier than the tumor diagnosis. Second, areas of gradual morphological transitions from the very bland meningioangiomatosis features to the perivascular hypercellular proliferation of clear-cut neoplastic cells at the edge of the tumor core could be identified, suggesting a progression from one component to the other. Finally, we found evidence of genetic diversity but continuity between the lesional components: The meningioangiomatosis showed clonal genetic imbalances, for example, 22 loss and 6q gain. The loss of chromosome 22 and the gain at 6q were shared with the tumoral lesions, which displayed additional gains and losses. In agreement with a previous study on meningioangiomatosis-associated meningiomas (16), overall our findings support the hypothesis that meningioangiomatosis is a clonal precursor lesion that may rarely undergo

malignant transformation following the occurrence of additional genetic events.

REFERENCES

1. Wang X, Haswell JR, Roberts CW. Molecular pathways: SWI/SNF (BAF) complexes are frequently mutated in cancer – mechanisms and potential therapeutic insights. Clin Cancer Res 2014;20:21–7
2. Agaimy A. The expanding family of SMARCB1(INI1)-deficient neoplasia: Implications of phenotypic, biological, and molecular heterogeneity. Adv Anat Pathol 2014;21:394–410
3. Allen JC, Judkins AR, Rosenblum MK, et al. Atypical teratoid/rhabdoid tumor evolving from an optic pathway ganglioglioma: Case study. Neuro Oncol 2006;8:79–82
4. Kleinschmidt-DeMasters BK, Birks DK, Aisner DL, et al. Atypical teratoid/rhabdoid tumor arising in a ganglioglioma: Genetic characterization. Am J Surg Pathol 2011;35:1894–901
5. Chacko G, Chacko AG, Dunham CP, et al. Atypical teratoid/rhabdoid tumor arising in the setting of a pleomorphic xanthoastrocytoma. J Neuro-oncol 2007;84:217–22
6. Kleinschmidt-DeMasters BK, Alassiri AH, Birks DK, et al. Epithelioid versus rhabdoid glioblastomas are distinguished by monosomy 22 and immunohistochemical expression of INI-1 but not claudin 6. Am J Surg Pathol 2010;34:341–54
7. Dougherty MJ, Santi M, Brose MS, et al. Activating mutations in BRAF characterize a spectrum of pediatric low-grade gliomas. Neuro Oncol 2010;12:621–30
8. Jeong JY, Suh YL, Hong SW. Atypical teratoid/rhabdoid tumor arising in pleomorphic xanthoastrocytoma: A case report. Neuropathology 2014;34:398–405
9. Miyahara M, Nobusawa S, Inoue M, et al. Glioblastoma with rhabdoid features: Report of two young adult cases and review of the literature. World Neurosurg 2016;86:515 e1–9
10. Yamamoto J, Takahashi M, Nakano Y, et al. Rapid progression of rhabdoid components of a composite high-grade glioma and rhabdoid tumor in the occipital lobe of an adult. Brain Tumor Pathol 2012;29:113–20
11. Nobusawa S, Hirato J, Sugai T, et al. Atypical teratoid/rhabdoid tumor (AT/RT) arising from ependymoma: A type of AT/RT secondarily developing from other primary central nervous system tumors. J Neuropathol Exp Neurol 2016;75:167–74
12. Bozzai B, Hasselblatt M, Turanyi E, et al. Atypical teratoid/rhabdoid tumor arising in a malignant glioma. Pediatr Blood Cancer 2017;64:96–9
13. Lach B, Kameda-Smith M, Singh S, et al. Development of an atypical teratoid rhabdoid tumor in a meningioma. Int J Surg Pathol 2017;25:567–72
14. Vaubel RA, Caron AA, Yamada S, et al. Recurrent copy number alterations in low-grade and anaplastic pleomorphic xanthoastrocytoma with and without BRAF V600E mutation. Brain Pathol 2018;28:172–82
15. Perry A, Kurtkaya-Yapicier O, Scheithauer BW, et al. Insights into meningioangiomatosis with and without meningioma: A clinicopathologic and genetic series of 24 cases with review of the literature. Brain Pathol 2005;15:55–65
16. Kim NR, Cho SJ, Suh YL. Allelic loss on chromosomes 1p32, 9p21, 13q14, 16q22, 17p, and 22q12 in meningiomas associated with meningioangiomatosis and pure meningioangiomatosis. J Neurooncol 2009;94:425–30
17. Rousseau G, Noguchi T, Bourdon V, et al. SMARCB1/INI1 germline mutations contribute to 10% of sporadic schwannomatosis. BMC Neurol 2011;11:9
18. Paulus W, Slowik F, Jellinger K. Primary intracranial sarcomas: Histopathological features of 19 cases. Histopathology 1991;18:395–402
19. Huether R, Dong L, Chen X, et al. The landscape of somatic mutations in epigenetic regulators across 1,000 paediatric cancer genomes. Nat Commun 2014;5:3630
20. Mack SC, Witt H, Piro RM, et al. Epigenomic alterations define lethal CIMP-positive ependymomas of infancy. Nature 2014;506:445–50